49th AIAA Aerospace Sciences Meeting including the New Horizons Forum and Aerospace Exposition
4 - 7 January 2011, Orlando, Florida

AIAA 2011-881

# Complementary Numerical and Experimental Data Analysis of the ETW Telfona Pathfinder Wing Transition Tests

Thomas Streit[1], Karl Heinz Horstmann[2]
*DLR,German Aerospace Center, 38108, Braunschweig, Germany*

Géza Schrauf[3]
*Airbus, D-28199 Bremen, Germany*

Stefan Hein[4], Uwe Fey[5], Yasuhiro Egami[6],
*DLR, German Aerospace Center, D-37073 Göttingen, Germany*

Jean Perraud[7]
*Onera Toulouse, 31055 France*

Itham Salah El Din[8]
*Onera Chalais-Meudon, 92320 France*

Ubaldo Cella[9]
*Piaggio Aero Industries, 80078 Pozzuoli (NA), Italy*

Jürgen Quest[10]
*European Transonic Windtunnel, D-51147, Cologne, Germany*

**Within the European Project Telfona the Pathfinder Model was designed, analyzed numerically, constructed and tested with the aim of obtaining a laminar flow testing capability in the European Transonic Wind Tunnel (ETW). The model was designed for natural laminar flow (NLF) for transonic flow conditions with high Reynolds number. Results of pre-test numerical analysis demonstrated that the Pathfinder wing pressure distribution was adequate for providing calibration test points. The ETW tests provided pressure distribution data while transition positions were determined from images using the Cryogenic Temperature Sensitive Paint Method (cryoTSP). The evaluation of this data with several transition prediction tools was used to establish the transition N-factor values for ETW. In this work, after-test CFD solutions are obtained using numerical Navier-Stokes solutions. In the first part of this work, numerical results are given which verify the requirements of the Pathfinder wing as a calibration model. In the second part, it is shown that for selected flow conditions a good agreement is obtained between stability analysis based on experimental and numerical data. In the third part the correlation of experimental transition locations to critical N-factors is summarized for ETW Test Phases I and II. In the fourth part numerical analysis and experimental data are used complementarily.**

[1] Research Scientist, Institute of Aerodynamics and Flow Technology, th.streit@dlr.de
[2] Research Scientist, Institute of Aerodynamics and Flow Technology, k.h.horstmann@dlr.de
[3] Expert Scientist, Senior Member AIAA, geza.schrauf@airbus.com
[4] Research Scientist, Institute of Aerodynamics and Flow Technology, stefan.hein@dlr.de
[5] Research Scientist, Institute of Aerodynamics and Flow Technology, uwe.fey@dlr.de
[6] Research Scientist, formerly DLR, now at Nagoya University, Nagoya Japan, y.egami@coe.mech.nagoya-u.ac.jp
[7] Research Engineer, Models for Aerodynamics and Energetics Depart., AIAA member, jean.perraud@onera.fr
[8] Research Engineer, Applied Aerodynamics Depart., itham.salah_el_din@onera.fr
[9] Senior Research Engineer, PHT Depart., ucella@piaggioaero.it
[10] Chief Aerodynamicist, Associate Fellow AIAA, jq@etw.de

## I. Introduction

The Telfona Pathfinder model was designed, analyzed numerically, constructed and tested to evaluate the possibility of laminar flow testing in the European Transonic Wind Tunnel (ETW). It was designed to allow natural laminar flow (NLF) at transonic, high Reynolds number flow conditions. Telfona (Testing for Laminar Flow On New Aircraft) is a European Research Project led by Airbus, which ended in 2009. The design and pre-test stability analysis for the Pathfinder wing was described in Ref. 1. The experimental data provided pressure distributions which are required to perform stability analysis. Transition locations were determined using Cryogenic Temperature Sensitive Paint Method (cryoTSP)[2]. Details of the wind tunnel tests are given in Ref. 3,4. The experimental data from the first and second Pathfinder ETW campaigns was processed and linear stability anlalyses were performed by Airbus[5]. The linear stability results show that data were sufficient to obtain critical ETW N-factors for cases with either predominant Tollmien Schlichting (TS) N-factors $N_{TS}$ or for predominant crossflow (CF) N-factors $N_{CF}$. The processed pressure distributions were then sent to the other Telfona partners DLR, CIRA, FOI, ONERA in order to perform stability analysis using several different methods. The analysis of this processed experimental data using local stability theory and database methods was summarized in Ref. 3,4. The present work completes the initial analysis of the third Pathfinder ETW campaign, presented in Ref. 6. Post-test CFD solutions have been obtained by Airbus/DLR, ONERA and Piaggio Aero for selected cases from all three campaigns. Numerical results are compared to the experimental ones and are used to complement the stability analysis.

The specifications of the Pathfinder wing are described in section 2. Section 3 describes the numerical methods used for CFD and stability analysis. Results are given in section 4. The results section has four parts. In the first part, CFD solutions are used to show the properties of the Pathfinder model. In the second part, numerical results for the pressure distribution and N-factors are compared to corresponding data obtained from the experiments. In the third part critical N-factor correlation results are summarized for ETW Test Phases I and II. In the fourth part, numerical solutions are obtained for the third ETW Pathfinder test campaign. No pressure distribution data exist for this test campaign. Using pressure distributions obtained numerically, and the TSP images from the ETW test, further cases were selected to complement the calibration of the critical ETW N-factors. Conclusions are given in section 5.

**Figure 1: Telfona Pathfinder Model in ETW wind tunnel test section.**

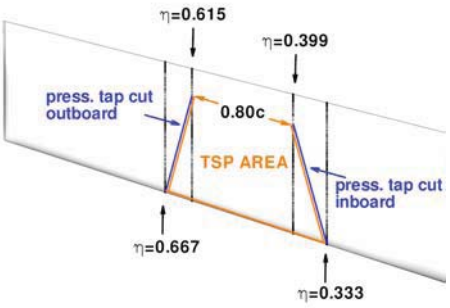


**Figure 2: Position of TSP patches and pressure tap sections.**

## II. Specifications of Pathfinder Wing

The Telfona Pathfinder model is a wing body configuration (see Fig. 1). The wing leading edge has a 18° sweep, span s and chord c are limited by wind tunnel size, i.e. s < 1.8m, c < 0.25m. Due to its small taper the Pathfinder wing planform looks like a rectangular swept wing. For the design it was required that the pressure distribution of spanwise sections should result in a linear variation of the amplification N-factor as function of chord position. Furthermore it was required that for the design point parallel isobars are obtained for a region which at least extends from 30% to 70% span, with transition occurring between 30% and 50% percent chord. It was designed for the expected N-factors ranges: $5< N_{CF}<8$, $6 <N_{TS}< 10$ (local stability theory, incompressible)[1]. The fuselage with belly fairing geometry is taken from an existing ETW model. The design point is M=0.78, Re=20 million, $C_L$=0.216. The relevant test flow conditions for the test section are: Ma=0.78±0.02, Re= 15 to 23 million, $T_{Tot}$= 117°K to ambient

temperature, $C_L$= 0.1 to 0.5, side slip β=0° and -4. The model has TSP patches on the upper and lower wing surfaces (see Fig. 1). Pressure taps are located on diagonal sections which are roughly located at normalized span positions η=0.33, 0.67 (Fig.2). Both the port and starboard wings are equipped with pressure taps.

## III. Mesh Generation, Numerical Methods

Meshes generated for this work are based on a CAD geometry obtained from the pre-test design geometry[1]. It is the same CAD geometry which was used to construct the wind tunnel model. CFD solutions are presented by DLR/Airbus, ONERA, and Piaggio Aero. DLR uses a hybrid unstructured mesh generated by Airbus. The mesh has 14.77 mil. points, with 3.93 mil. tetrahedra, and 27.94 mil. prisms. RANS solutions are obtained using the DLR-TAU-code[7]. For turbulence modelling the algebraic Spalart Allmaras model is used as well as the 2 equation SST model. Solutions are obtained with a full turbulent layer and fixed transition. Piaggio Aero generated a structured mesh with 15 millions hexahedral cells. The wing surface has 101 sections spanwise, each with 451 points in chord direction. RANS solutions are obtained using the CFD++ code[8]. The q-ω SST turbulence model is used for fully turbulent solutions. ONERA used the structured Piaggio mesh. RANS solutions are obtained using the ONERA elsA code[9] in turbulent mode, with the Spalart-Allmaras model. In addition, ONERA/Airbus, created a new structured mesh, with about 23 millions cells. For this mesh, elsA solutions were obtained with the 2 equation SST model.

Stability theory was performed in successive steps with several modelling levels. The first step aimed at calibrating the N-factor methods for ETW and verifying the coherence of available data. It is based on pressure distributions recorded in the ETW test campaigns and is described in Ref. 3-5. In this work a second step was performed, stability analysis was performed using numerical pressure distributions in addition to experimental pressure distributions. The stability analysis was based on linear stability theory using the LILO[10] code (with exact stability code and database methods) and the CASTET code[11] (exact stability methods) and the ONERA database method[12,13]. Stability analysis for pressure distributions obtained with the DLR-TAU and the CFD++ RANS solutions was performed using LILO. LILO is embedded in the STABTOOL program. In STABTOOL the three programs: PREPCP, COCO and LILO are used sequentially. PREPCP pre-processes the input pressure distributions in order to prepare them for boundary layer calculation. COCO performs compressible boundary layer calculation for the stability analysis, which is performed by LILO. LILO uses a $N_{TS}/N_{CF}$ method, in which $N_{TS}$ is obtained by using the constant wave angle ψ strategy at frequencies covering the complete range of unstable waves, and $N_{CF}$ is obtained by considering only stationary instabilities, using either the constant wavelength strategy or the constant spanwise wavenumber $\beta^*$ strategy. LILO results were obtained for incompressible $N_{TS}/N_{CF}$ factors. Stability analysis results for elsA and CFD++ pressure distributions were obtained using the CASTET code and the ONERA data base method. Compressible $N_{TS}/N_{CF}$ and envelope method results were obtained. Boundary layer quantities were computed using the 3D boundary layer code 3C3D. In the first and second step the ETW was calibrated for N-factors, using complementarily experimental data and CFD solutions, which is the aim of this work. Once obtained, the calibrated N-factors can be used to obtain CFD solutions with automatic transition prediction using internal stability prediction tools. Internal stability predictions tools have been implemented in the TAU code[14] and in the elsA[13,15] code with the aim to predict transition lines for complete aircraft configurations[16]. Here, in a third step the use of automatic transition prediction is illustrated for the Telfona Pathfinder configuration with elsA solutions. These solutions are obtained on the refined mesh with 23 millions cells. Transition is predicted using the compressible AHD criterion[17] for TS transition, and C1 criterion[17] for crossflow.

In this work the boundary-layer profiles used for stability analysis were usually computed assuming adiabatic wall temperature boundary conditions. However, in order to assess the wall temperature influence additional boundary-layer computations with a prescribed wall temperature distribution were performed. In the latter study a boundary-layer code based on a code described in Ref. 18 was used which assumes infinite swept wing conditions. Differences in the boundary-layer profiles obtained by the COCO code which assumes conical flow and those obtained based on the infinite swept wing assumption are small since the Pathfinder wing has a tapering ratio nearly equal to 1. For studying the effect of the wall temperature on the N-factors the linear version of the stability and transition analysis code NOLOT[19] was used.

## IV. Results

Stability analysis and CFD results are given in this section. In the first subsection the CFD solutions are analyzed regarding the specification of the Pathfinder model and its usefulness for stability analysis. In the second subsection numerical results are compared to experimental data from ETW Phase I and II. In the third subsection the correlation of experimental transition locations to critical N-factors is summarized for ETW Test Phases I and II. In the fourth subsection numerical and experimental results are used complementarily to analyse ETW Phase III.

### A. Properties of the Pathfinder model

TAU-RANS solutions for two flow condition are given in Fig. 3 to illustrate the parallel isobar concept of the Pathfinder wing. Pressure distributions are shown for sections η=0.33 and η=0.67. Flow conditions are M=0.78, Re=20 million and two values of $C_L$, 0.208 and 0.320 are selected. The solution at $C_L$=0.208 is compared to the original design solution given in Ref. 1, which showed perfect parallel isobars within the desired spanwise limits. Here there is a good agreement with the original target for the lower side, whereas for the upper part differences are obtained in the sensitive transonic region, especially at the shock position. After excluding some of the possible causes for these differences it was concluded that they may be attributed to small geometry oscillations between the definition sections, which originated in the CAD construction process and to a smaller extent to mesh refinement differences in the solution. Parallel isobars are also obtained at higher incidences on the upper side.

Figure 4 demonstrates that the Pathfinder pressure distribution is relatively independent of the turbulence models used and of fixing or not the transition point. In order to see the differences more clearly the pressure distributions are plotted in a region extending from the nose up to the pressure minimum. The turbulent boundary layer was modelled with the 1 equation SA model or with the 2-equation SST model. Transition position was fixed at x/c=0.6. Since the solutions show insensitivity of Cp to transition position and turbulence model it was decided to obtain the rest of the TAU solutions within this work (if not indicated) by fixing transition at x/c=0.6 and using the 2-eq. SST model

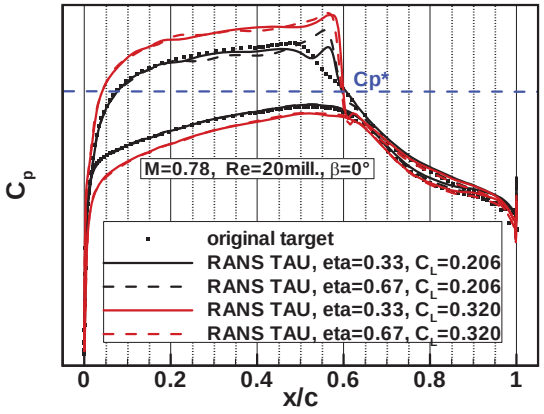


**Figure 3. Pressure distributions for TAU-RANS solution illustrating isobar concept.**

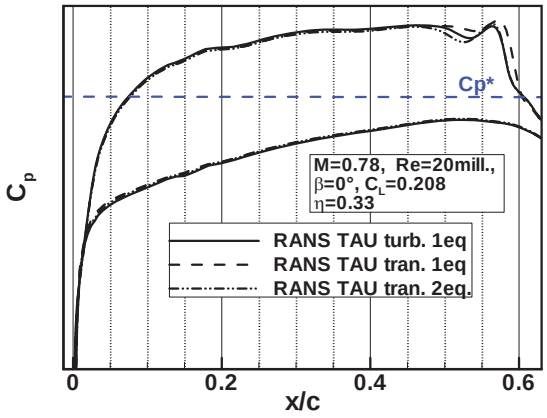


**Figure 4. Sensitivity of solution to selected turbulence model and transition position**.

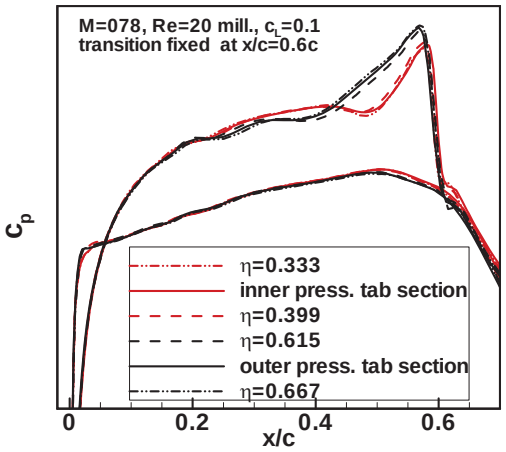


**Figure 5. Spanwise variation of pressure distribution. Flow condition: M=0.78, Re/$10^6$=20, $C_L$=0.1.**

Stability analysis in this work is based on pressure distribution input. The pressure distributions at a constant span section are used to compute longitudinal and transversal boundary layer data using the conical assumption. The latter assumes that in the spanwise direction pressure distribution does not vary along constant normalized chord positions. For the Pathfinder model this requirement is satisfied also for off design flow conditions as shown in Figure 5. For this case on the lower side the parallel isobar concept is also achieved.

In Fig. 6 a comparison of stability analysis is shown for RANS Cp-distributions solutions obtained with the TAU and the CFD++ codes. Stability analysis was performed using the LILO code. Flow conditions are M=0.78, Re=18 million, $C_L$=0.1. There is a good agreement in the pressure distribution. Effective sweep angle[20] was obtained from the CFD solutions. Results for $N_{CF}$-factor are closer together than for $N_{TS}$-factors.

### B. Comparison of experimental and numerical results

RANS solutions were obtained for ten cases from the first and second ETW Telfona Pathfinder test campaigns. Selected cases included the typical flow condition. In addition to the experimental data, they provided a numerical pressure distribution database to perform stability analysis. Stability analysis may then be based on ETW, TAU-RANS and CFD++ pressure distributions. Flow conditions for these cases are given in table 1.

| Case | ETW Test No. | CFD method | $Re/10^6$ | $T_{Tot}$[°K] | $C_L$ | M | β[°] |
|---|---|---|---|---|---|---|---|
| 1 | P079, P080 | TAU, elsA | 20 | 175 | 0.00 | 0.78 | 0 |
| 2 | P081, P085 | TAU,CFD++ | 20[+] | 175 | 0.10 | 0.78 | 0 |
| 3 | P086, P087 | TAU | 20 | 175 | 0.21 | 0.78 | 0 |
| 4 | P088, P089 | TAU, elsA | 20 | 175 | 0.32 | 0.78 | 0 |
| 5 | P090, P091 | TAU | 20 | 175 | 0.401 | 0.78 | 0 |
| 6 | P092, P093 | TAU | 20 | 175 | 0.498 | 0.78 | 0 |
| 7 | P251, P251 | TAU | 15 | 175 | 0.45 | 0.78 | 4 |
| 8 | P254, P255 | CFD++ | 10 | 175 | 0.46[*],0.45[**] | 0.78 | 0 |
| 9 | P256, P257 | TAU | 10 | 175 | 0.45 | 0.75 | 0 |
| 10 | P268, P269 | CFD++ | 10 | 175 | 0.10 | 0.78 | 0 |

**Table 1: Flow conditions for selected cases.** [*]ETW, [**]RANS. [+]For case 2 the CFD++ results were obtained at Re=18 million but stability analysis was performed at 20 mil. The first ETW test number corresponds to $C_p$ measurement, the second corresponds to the TSP measurement. In the last column β is the yaw angle.

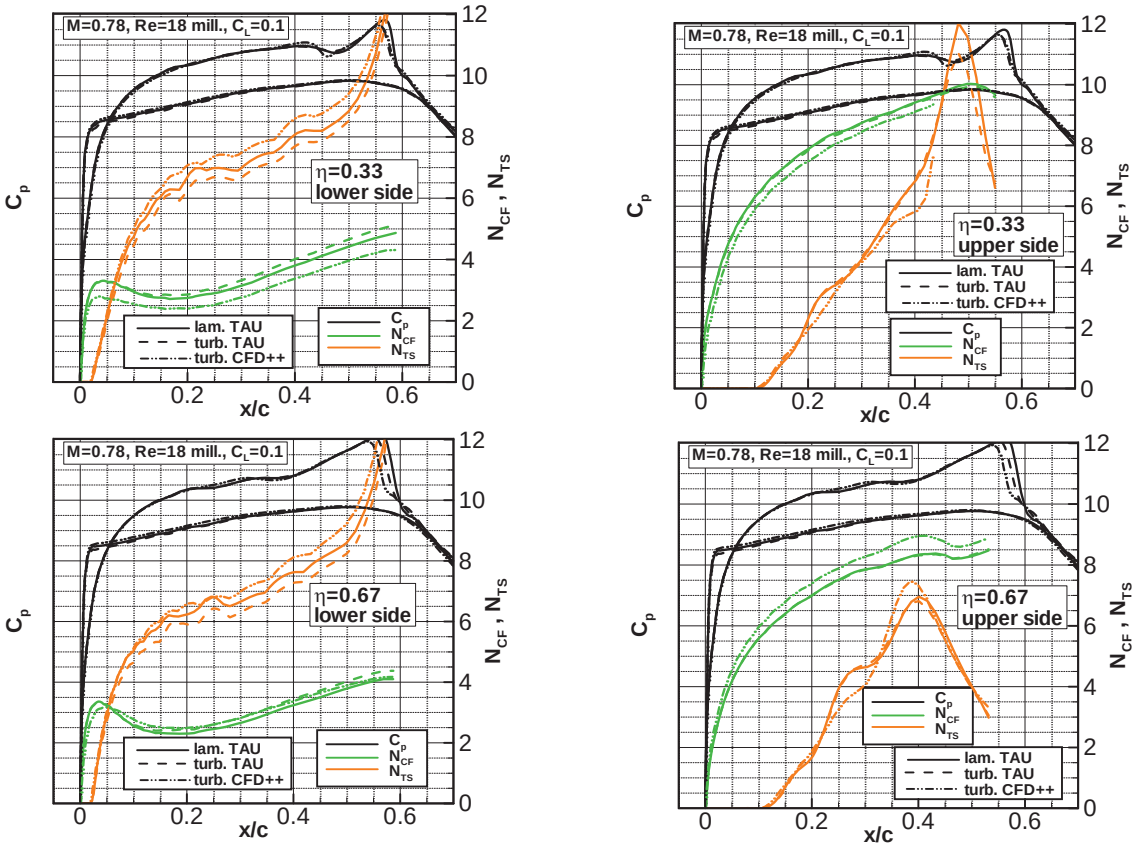


**Figure 6. Pressure distributions and stability analysis for RANS solution obtained with CFD++ and TAU.**

Data are compared at two sections with span=0.33 and 0.67 for upper and lower surface. For the experimental results the figures include data for the corresponding starboard and port wing section. Especially for the $N_{CF}$-factor the effective sweep plays an important role. For most experimental cases effective sweep was predicted with sufficient accuracy indicating that the number of pressure taps in the stagnation line area is sufficiently dense.

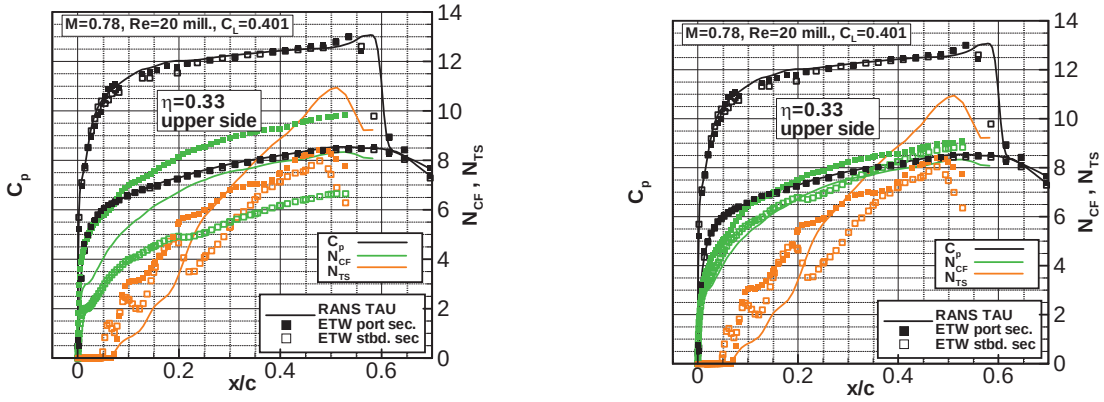


**Figure 7. Comparison of experimental and numerical stability analysis results for case 4 upper side. Left side with non averaged and right side with averaged experimental effective sweep.**

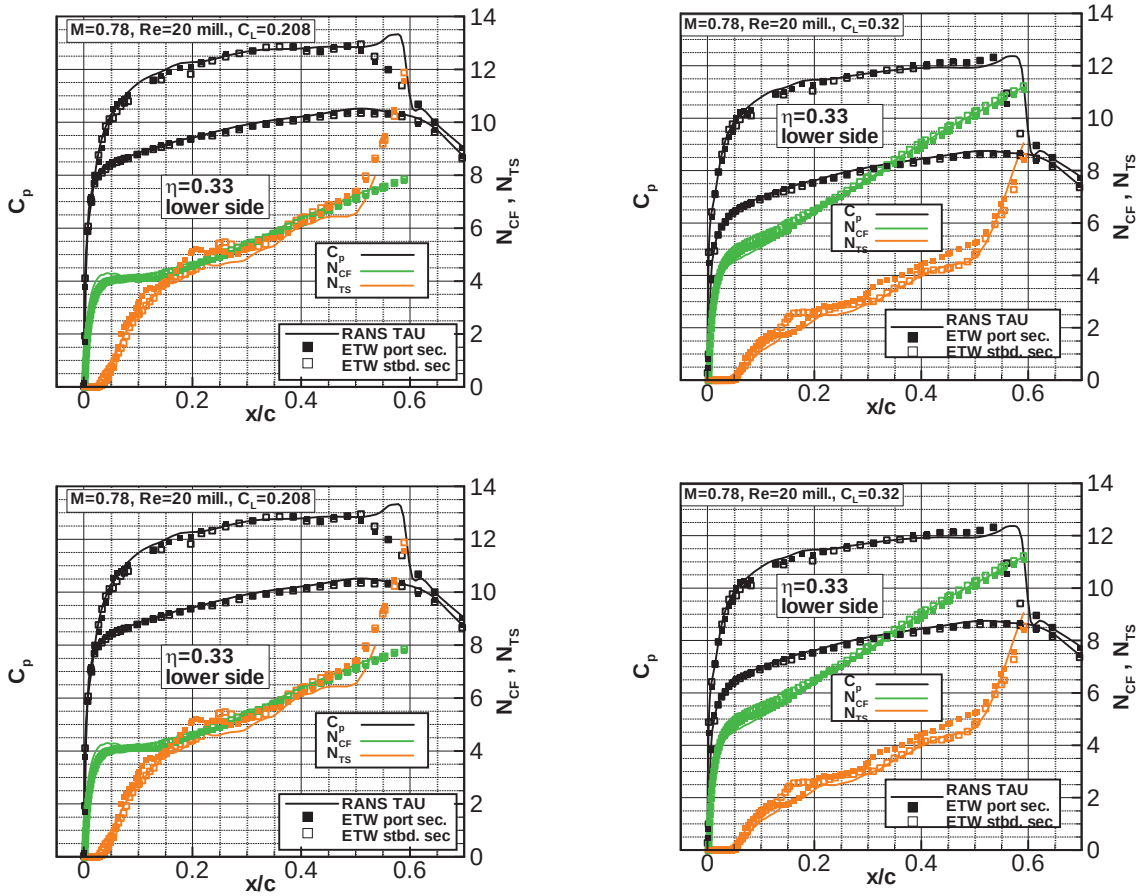


**Figure 8. Comparison of experimental and numerical stability analysis. Results for lower side inboard section for case 3 (left) and case 4 (right).**

Except for cases 3, 5 and 7, the effective sweep angle used for stability analysis was the one obtained by the pre-processing tool PREPCP. For the experimental cases 3 and 5, the effective sweep angle showed some scattering among the sections. In the cases of zero yaw, to improve the results the average of the experimental values obtained for all 4 sections (2 for port wing and 2 for starboard wing) were taken. Figure 7 compares results with averaged and non-averaged effective sweep for case 5, for which differences between port and starboard wing were largest. Note that the effective sweep angle coming from the CFD solution could also be used.

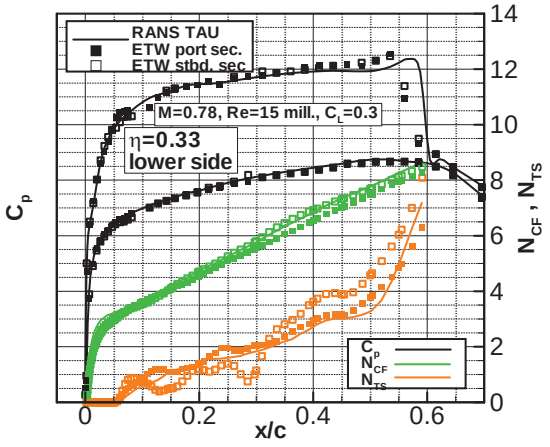


**Figure 9 Comparison of experimental and numerical stability analysis. Results for lower side inboard section for ETW Test No. 223 using pressure distributions from case 4.**

The comparison of stability analysis for numerical and experimental pressure distributions for cases 2-6 and 10 is given in Ref. 6. The agreement between N-factors based on numerical and experimental pressure distributions is good, in some cases very good (section $\eta$=0.33, lower side, cases 3-5,10). Figure 8 shows results for cases 3 and 4, for $\eta$=0.33, lower side. Differences are in some cases larger for $N_{TS}$ (e.g: section $\eta$=0.33, upper side, case 5, see Fig.7) than for $N_{CF}$, but it is of the same order of magnitude as the difference between corresponding experimental $N_{TS}$ data from port and starboard wing sections. Since the numerical solution for the pressure distribution is smoother in the nose region, $N_{TS}$-differences also occur at the nose region (x/c< 0.2). However $N_{TS}$ is small for this region.

The computed RANS solutions can be used to obtain stability analysis for several additional test cases, with the same flow condition except for slightly different Reynolds number. For such cases the numerical pressure distribution with similar flow conditions are used but boundary layer input for stability analysis is computed with the correct Reynolds number. This is illustrated in Fig. 9 for ETW Test No. 223. This test has similar flow conditions as case 4, but a different Reynolds number. Flow conditions are M=0.78, $C_L$=0.33 but Re=15 million As shown in Fig. 9, despite the fact that the difference in Reynolds number is not small, the numerical pressure distribution and its stability analysis agree.

### C. Correlation and classification of cases

Critical N-factors are obtained by correlating the transition position obtained in the TSP-image with the $N_{TS}$, $N_{CF}$ values which the stability analysis provides for that transition position. According to the critical N-factors values the transition is classified in three types, CF-case, TS-case and mixed case. For the CF-case, $N_{TS}$ is small, for the TS-case $N_{CF}$ is small and for the mixed case both $N_{TS}$ and $N_{CF}$ are significant. This classification can be applied for cases in which transition occurs before a predicted laminar separation. There are cases where transition occurs after a laminar boundary layer separation, while the critical N-factors have not been reached. Transition may occur right after the shock on the suction side or past the pressure minimum on the pressure side. In those cases, the boundary layer code often predicts a laminar separation at a position upwind from the observed transition position. The corresponding TSP images from these cases can be used to give a relative correlation, i.e. the critical $N_{TS}$, $N_{CF}$ values are higher than the N-factors at the position at which laminar separation is predicted. Another aspect is that extremely thin boundary layers are observed at large Reynolds numbers. At M=0.78, $Re/10^6$=20 on the Pathfinder inboard section, the boundary layer thickness is typically 40 to 60 μm for 2% < x/c < 5%. Therefore tiny impurities can lead to turbulent wedges. A classical roughness estimate indicates that with the above laminar boundary layer thickness, critical roughness size is about one order of magnitude less. Due to turbulent wedges some of the correlated CF, TS or mixed transitions only provide a relative correlation. It was observed, that for TS cases, turbulent wedges more often prevented a clear transition line, than for CF cases. Figures 10-14 show selected TSP-images and corresponding pressure distributions and stability analysis, for CF, TS, mixed transition, transition at shock and after pressure minimum. Note that for the TS case (Fig.11) and mixed transition case (Fig. 12) only a relative correlation is possible. Correlations were done using the stability analysis for the experimental pressure distributions. For shown cases there is a good agreement between experimental and numerical values. In the correlation, additional RANS solutions are used as a guide to indicate if the effective sweep is correct, or if other discrepancies occur which have to be corrected or may lead to discard the considered case.

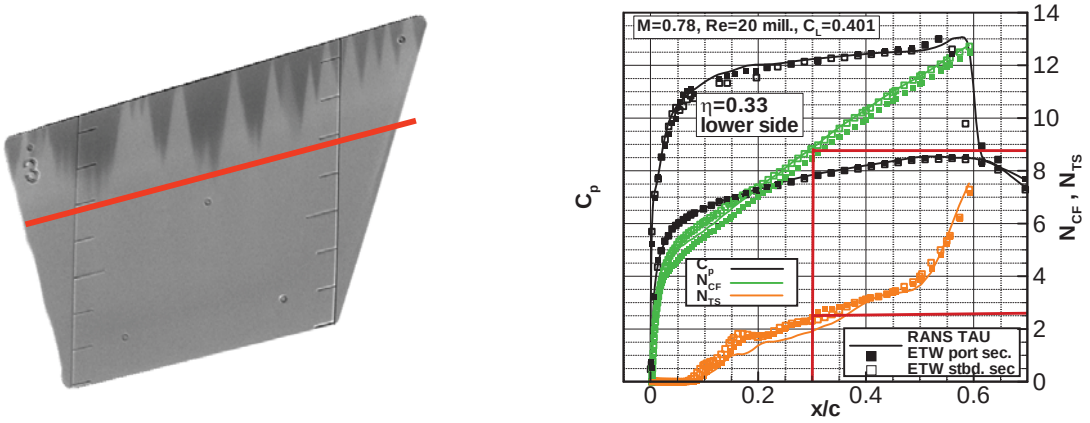


**Figure 10 CF-transition case. ETW Test No. 090, at the left TSP image, at the right stability analysis and critical N-factors. Red lines indicate transition position and N-factor correlation.**

For the classification of correlation three numbers were introduced. The first is an integer $N_{type}$, it takes values 1 to 5 according to the 5 transition types, given in Fig. 10 to 14. Furthermore a Number $N_I$ was introduced which takes values 1 or 0, if either a definite or a relative correlation can be performed. A third number $N_u$ was introduced to indicate if the correlation is usable, it takes values 0 (not usable), 0.5 (uncertain or not understood) and 1.0 (usable). The value $N_u$ =0.5 was mostly assigned to cases where TS-transition occurred at a position close to the nose. For these cases the resulting critical $N_{TS}$ factors reached nearly free flight critical values, i.e. the turbulence level of the wind tunnel seemed not to influence transition. The value $N_u$ =0.5 was also assigned to cases where the pressure distribution leads to a steep N-factor growth in the transition area, therefore decreasing the accuracy in N-factor correlation. Not usable cases are such where the following happens: too many wedges or relative correlated critical N-factors too low. Cases where a relative correlation results in critical N-factors, with both $N_{TS}$ and $N_{CF}$ values lower than seven, were discarded, since good quality correlations from other measurements have indicated that critical N-factors are higher than these values.

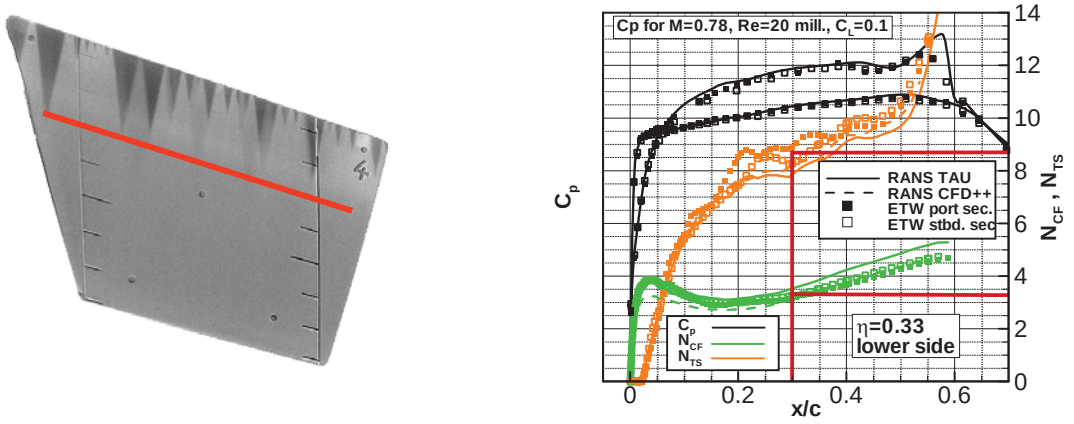


**Figure 11 TS-transition case. ETW Test No. 081, TSP image (left), stability analysis and critical N-factors (right). Red lines indicate transition position and N-factor correlation.**

The input data for stability analysis based on experimental pressure distribution was created by Airbus and DLR independently in order to reduce error sources. RANS pressure distributions for stability analysis was provided by Airbus/DLR, Piaggio, and ONERA. For Test Phase I, 10 cases were considered for stability analysis. In Test Phase II, stability analysis was performed for 18 cases (due to similar flow conditions this corresponds to 22 ETW measurements in which TSP Images were taken). The correlation for both Phases provided a total of 20 usable correlations with $N_i$=1. A total of 39 correlations were obtained for cases where transition occurred before shock or pressure minimum (i.e $N_{type} \leq 3$) with $N_i$=2. An additional 40 usable cases were obtained for relative correlation and transition after the shock or pressure minimum, ie. $N_i$=2, $N_{type}$=4,5. Further 11 correlations were obtained with $N_u$=0.5.

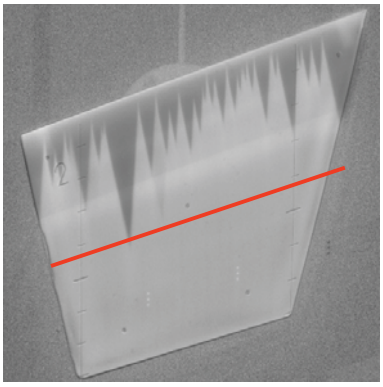

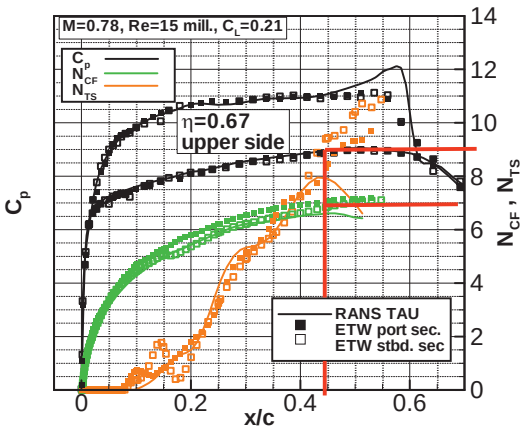


**Figure 12. Mixed-transition case. ETW Test No. 222, TSP image (left), stability analysis and critical N-factors (right). Red lines indicate transition position and N-factor correlation.**

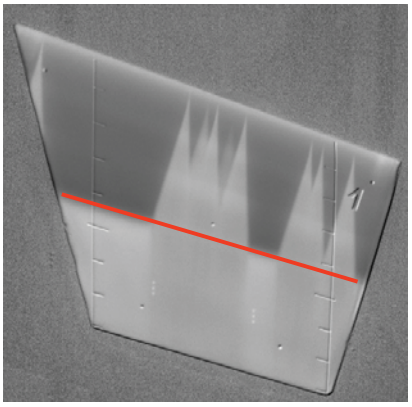

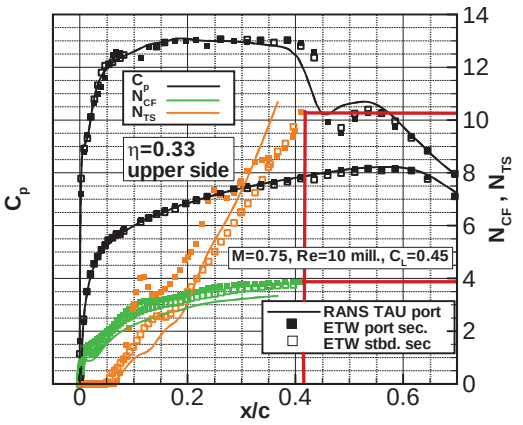


**Figure 13 Shock Transition case. ETW Test No. 257, TSP image (left), stability analysis and critical N-factors (right). Transition at upper surface was fixed at shock position. Red lines indicate transition position and N-factor correlation.**

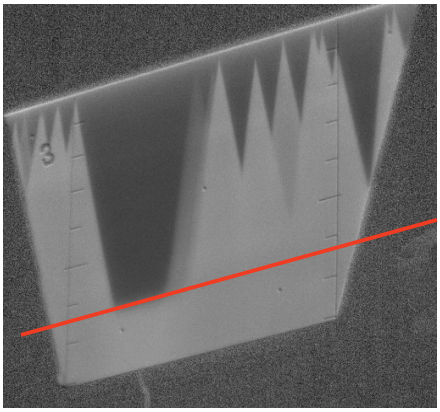

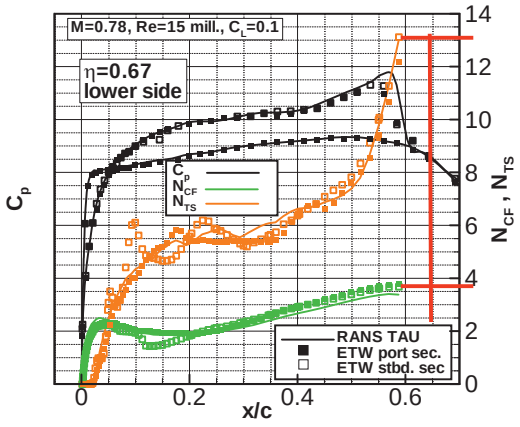


**Figure 14 Transition after pressure minimum. ETW Test No. 221, TSP image (left), stability analysis and critical N-factors (right). Red lines indicate transition position and N-factor correlation.**

### D. Results for ETW Pathfinder Phase III test campaign

.

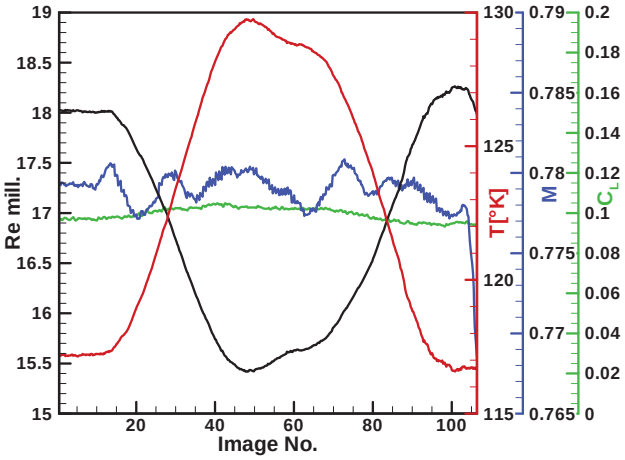


**Figure 15. Change of flow conditions for Test No. 699**.

TSP data and pressure distributions from test campaigns I and II have been used to obtain transition critical N-factors (see Ref. 3,4,6 and previous section). For ETW Phase III, TSP data exists but pressure distributions were not recorded. Therefore, CFD based pressure distributions are required to analyse these cases. TSP images exist for the whole temperature step up/step down-recording process. Within the temperature step up/step down-recording process the Re number changes accordingly. Variations in Mach number and $C_L$ are small since it is tried to keep them constant. Due to the Reynolds number variation, the transition changes its position in the corresponding TSP images. Therefore ETW Phase III offers several new cases with possible multiple correlations within one ETW Test. An example of a step up/ step down measurement is given in Fig. 15, where variation of flow variables is shown for ETW Test No. 669. Corresponding TSP images for maximum and minimum Re numbers for this ETW Test No. are given in Fig. 16 for the upper side. They show a transition at the shock position located at 0.60c for Re=15.4 million and a CF transition for 0.25-0.30c at Re=18.1 million.

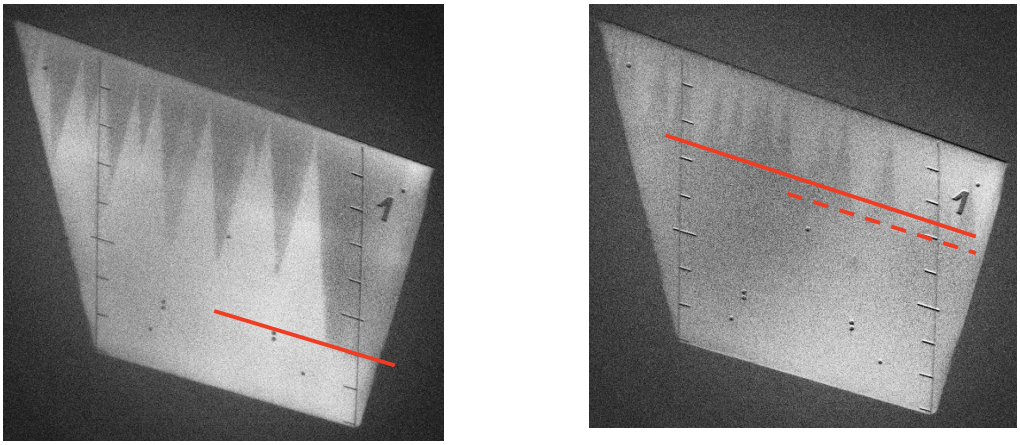

**Figure 16. ETW Test No. 699: TSP Images for upper wing at maximum (right) and minimum (left) Re number for temperature step up/down measurement.**

Figure 17 shows stability analysis based on TAU-RANS pressure distributions. Solutions are obtained at the ETW Test No. 699 minimum and maximum Re number. Flow conditions are: M=0.78, Re=18.1 million, $C_L$=0.095, $T_{total}$=116.58K and M=0.78, Re=15.4 million, $C_L$=0.1032, $T_{total}$=129.74K. The TSP images indicate that for minimum Re number, transition at the outboard section occurs at 60% (pressure minimum). For maximum Re-number the CF transition at 0.25c to 0.30c correlates to an $N_{CF}$ value varying between 8.8 and 9.2 for the inboard section and $N_{CF}$ value varying between 8.2 and 8.5 for the outboard section. The results obtained with CFD ++ and TAU for the flow condition M=0.78, Re=18.1 million and $C_L$=0.1 which have been compared in Fig. 6 have flow conditions close to the maximum Reynolds case from ETW Test No. 699. In the region of transition indicated by the TSP methods both numerical methods differ in $N_{CF}$ and $N_{TS}$ by a value $\Delta N_x \approx 0.5$ (see Fig. 6).

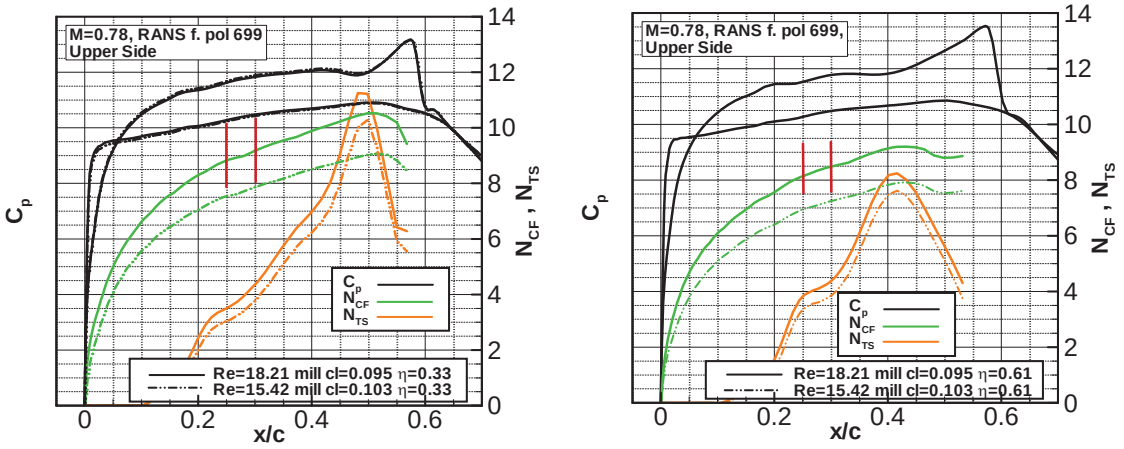


**Figure 17. ETW Test No. 699: Upper wing stability analysis results for numerical solutions at maximum and minimum Re number for temperature step up/down measurement. The left side shows results at the inboard section and the right side shows results for the outboard section. Red lines correlate transition position from the TSP images for the maximum Re number case.**

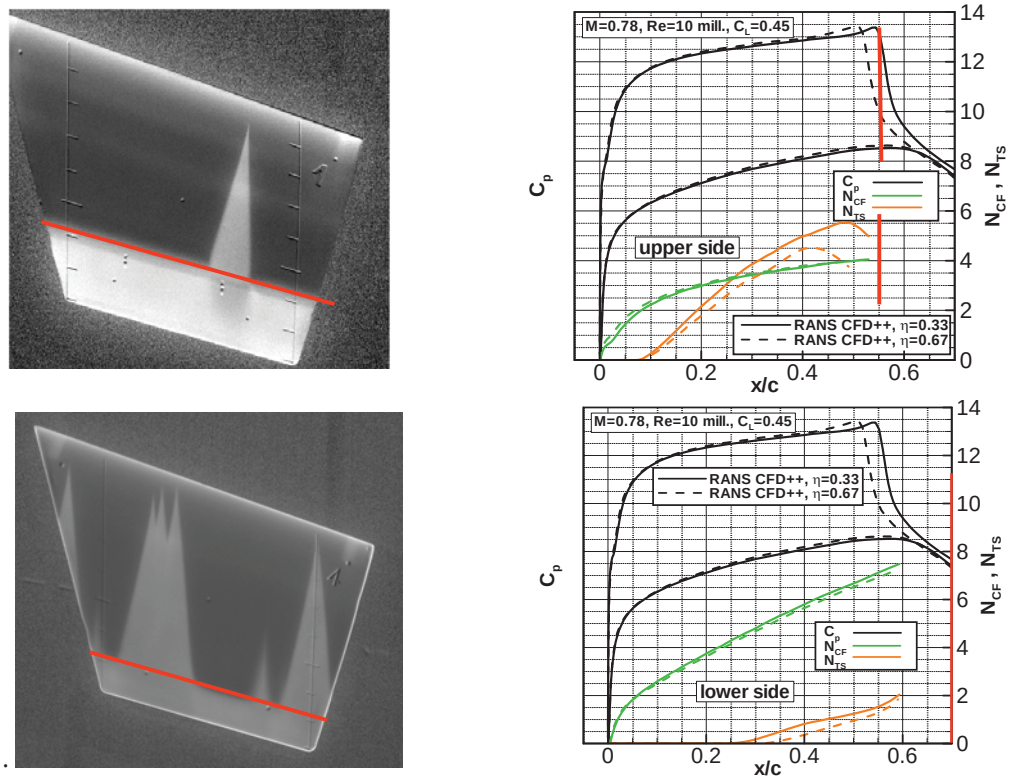


**Figure 18. TSP image and stability analysis for flow conditions corresponding to ETW Tests No. 710, 747, 793, 794 (also 255 Phase II)**

Figure 18 shows stability analysis for M=0.78, Re=10 million, $C_L$=0.45 and a corresponding TSP image from ETW Test No. 794. Transition occurs at the shock for the upper side and after pressure minimum for the lower side.

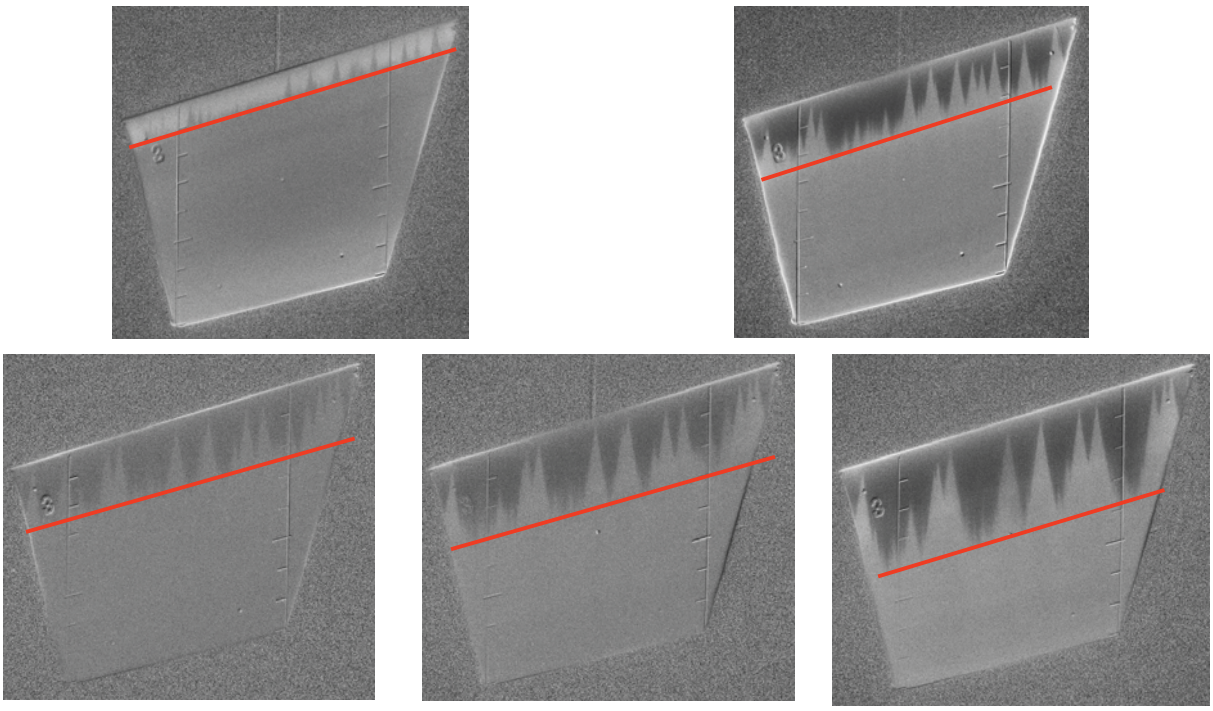

**Figure 19. Selected TSP images for ETW Tests No. 697 & 769 with M=0.78 and $C_L$ close to 0.45. Upper side TSP images for Pol. 769, $Re/10^6$=23.0 (left) and $Re/10^6$=19.75 (right). Lower side TSP images for Pol. 697, $Re/10^6$=17.4 mil. (left), $Re/10^6$=16.9 (middle), $Re/10^6$=16.0 (right).**

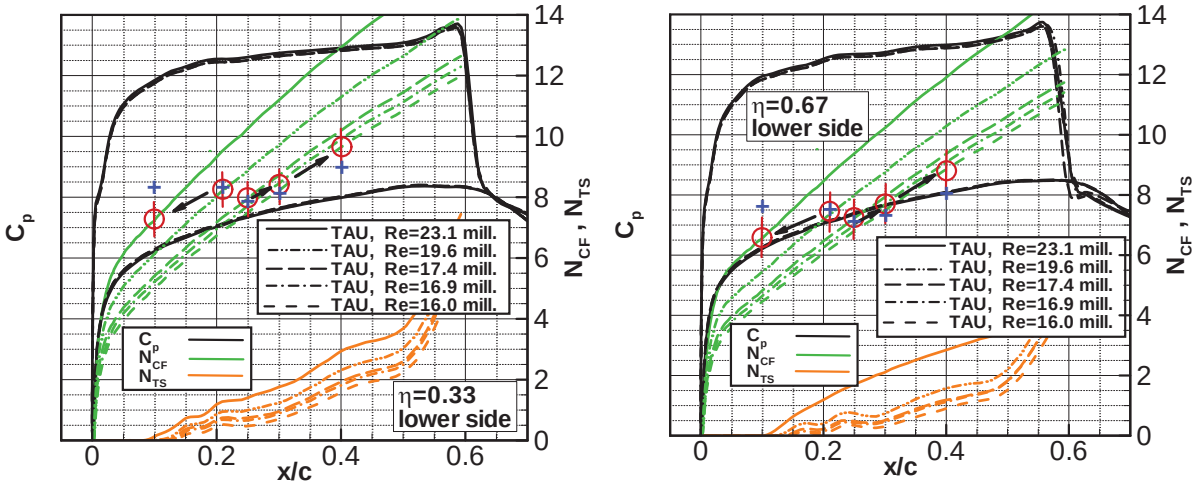


**Figure 20. Lower wing stability analysis results for numerical solutions for ETW Tests No. 697 & 769. Solutions correspond to TSP images given in Fig. 19. Red circles correlate $N_{CF}$ values at transition position from the TSP images. Black arrows between correlations indicate the sequence in which measurements were performed. Blue symbols are estimated corrections to the correlations due to wall temperature influence.**

Another useful example for correlation is given in Fig. 19 which shows TSP images indicating the evolution of CF dominated transition at the lower side for $C_L$=0.45 as function of Re-number. TSP images are taken from ETW Test No. 769 and ETW Test No. 697: Corresponding CFD solutions are given in Fig.20. The stability analysis for Re=19.6 million, is based on pressure distribution results for Re=23.1 million and Re=17.4 million. The circles

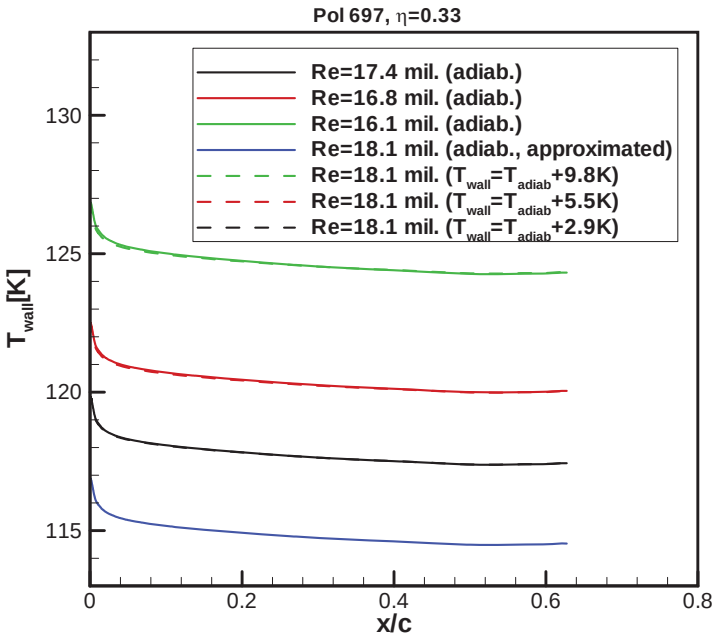


**Figure 21. Adiabatic wall temperature for selected ETW Test No. 697 temperature step up case. Shown are adiabatic wall temperature conditions for Re/10$^6$= 16.1, 16.8, 17.4 in comparison to Re/10$^6$=18.1 adiabatic wall temperature plus constant offset temperature.**

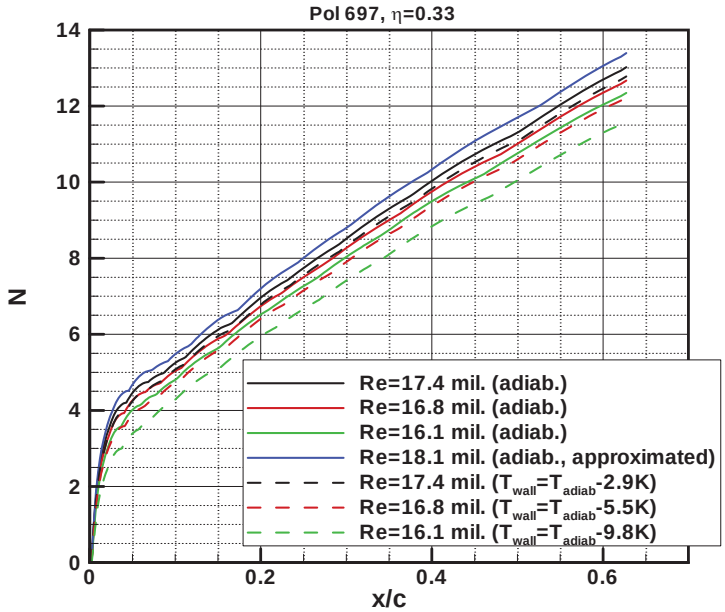


**Figure 22. Crossflow compressible N-factor for ETW Test No. 697 temperature step up case. Solutions for adiabatic wall temperature and colder wall with constant temperature offset relative to adiabatic wall temperature.**

indicate the CF correlation. Black arrows indicate the sequence in which measurements were performed. In the case of ETW Test No. 769, the two correlated points were measured in a temperature step down sequence. The less stable correlated value for the higher Reynolds number may be attributed to wall temperature effects. A warmer wall temperature in comparison to the adiabatic temperature destabilizes the boundary layer.

In the case of ETW Test No. 697 the three correlated points were measured in a temperature step up sequence. The more stable correlated values at the final lower Reynolds number may be also attributed to wall temperature effects. In this case the colder wall temperature stabilizes the boundary layer. All CFD solutions in this work were obtained using as wall temperature the adiabatic temperature and this was also assumed in the boundary layer calculations for stability analysis. To study the influence of wall temperature, stability analysis was performed for ETW Test No. 697 assuming wall temperature colder than the adiabatic one. Using the pressure distribution obtained from the CFD solution, compressible boundary layer quantities were computed by specifying the wall temperature distribution. The β=const. N-factor integration strategy together with local compressible stability theory was used to compute the N-factors for stationary crossflow modes with the NOLOT code. For the beginning of the ETW Test No. 697 temperature step up measurement flow conditions were: Re/10$^6$=18.1, total temperature=117.2K. First the adiabatic wall temperature was determined as function of x/c for the flow conditions at the beginning of the temperature step up measurement. As shown in Fig. 21 the adiabatic wall temperature for the flow conditions corresponding to Re/10$^6$= 16.1, 16.8 and 17.4 differs to the adiabatic wall temperature for Re/10$^6$=18.1 by an approximately constant temperature difference. To study the effect of wall temperature influence, it is now assumed that the wall temperature distribution during the temperature step up measurement is constant and given by the

initial Re=18.1 million condition. Stability results are given in Fig. 22 for section η=0.33. The assumed colder wall temperature stabilizes the boundary layer. In a similar way, results with specified wall temperature were obtained for the outboard section and for ETW Test No. 769. For the latter case, measurement was modeled by specifying a wall temperature distribution warmer than the corresponding adiabatic one. $N_{CF}$ results with specified wall temperature show a destabilizing effect. For this pressure distribution and flow conditions, the change in compressible $N_{CF}$ due to a wall temperature offset is approximated by $\Delta N \approx 0.079K^{-1} \cdot \Delta T_{wall}$. Compressible to incompressible corrections are very small. Corrections to the correlated $N_{CF}$ values for ETW Test No. 697 and 769, based on this approximation are shown in Fig. 20. The corrections reduce the scattering in the correlated $N_{CF}$ values.

Selected Phase III cases were presented. Evaluation of all Phase III cases has added further 33 usable correlations to the 99 correlations mentioned in subsection C. Some of them are valuable because they provide critical factors in regions of $N_{CF}$-$N_{TS}$ space not correlated neither in Phase I nor II.

Further cases from the third ETW test campaign were also analyzed by ONERA, using the elsA solver to obtain RANS solutions[6]. The calibration of the critical N-factor for the stability methods used by ONERA was completed with new correlations. Here, elsA results are presented, which predict transition using the calibrated N-factors. For that purpose, a new 23 million points structured mesh was prepared by Airbus, ensuring about 50 points in the boundary layer and a chordwise distribution compatible with the indirect estimation in elsA of the incompressible shape factor used in the ONERA transition prediction criterion for TS transition. This mesh was designed in order to allow direct comparison of elsA's results with 3C3D's. The compressible version of the ONERA AHD criterion[17] was used, together with the C1 criterion[17] for crossflow, to directly test the transition prediction capability of elsA[15] and compare it to the experimental results. The AHD criterion is an extended version of the Granville criterion, based on stability calculations, and the C1 criterion is an empirical one based on the crossflow displacement thickness. Cases 769 and 787 were considered and 787 is presented here in Fig. 23.

In the left part of the figure, results obtained with 3C3D based on elsA's (turbulent) mean flow are first presented. The blue curve has been obtained with the $N_{CF}/N_{TS}$ approach with transition N-factors calibrated from the previous cases[4] ($N_{CF}$ = 16, $N_{TS}$ = 6). Note that in this case $N_{CF}$ is based on propagating waves ($f \geq 0$) and not only on stationary disturbances). The second curve is obtained using the compressible AHD for TS transition and the C1 criterion in 3C3D. In this case, transition moves slightly upstream, and for this crossflow case is independent of the turbulence level. It can also be seen that the crossflow transition detected using C1 shows a tendency to jump up or down at some locations, although the average line is quite acceptable. This is a typical behavior of the C1 criterion, giving acceptable values but being much less robust than methods based on stability analysis.

In the right picture, the transition line obtained with 3C3D and the AVJ criterion, and that obtained with the transition prediction tools inserted inside the elsA code are drawn. In case of elsA, the trans-shift value is large and has the effect of delaying the impact of transition on the boundary layer with respect to the previous result drawn on the left side. The approach used here consists in imposing a delay between transition detection and the start of turbulence with the effect of improving robustness, in order to avoid oscillations of the transition location which may appear without this delay. It also has the effect of reducing the distance that was visible between the two transition lines on the left side.

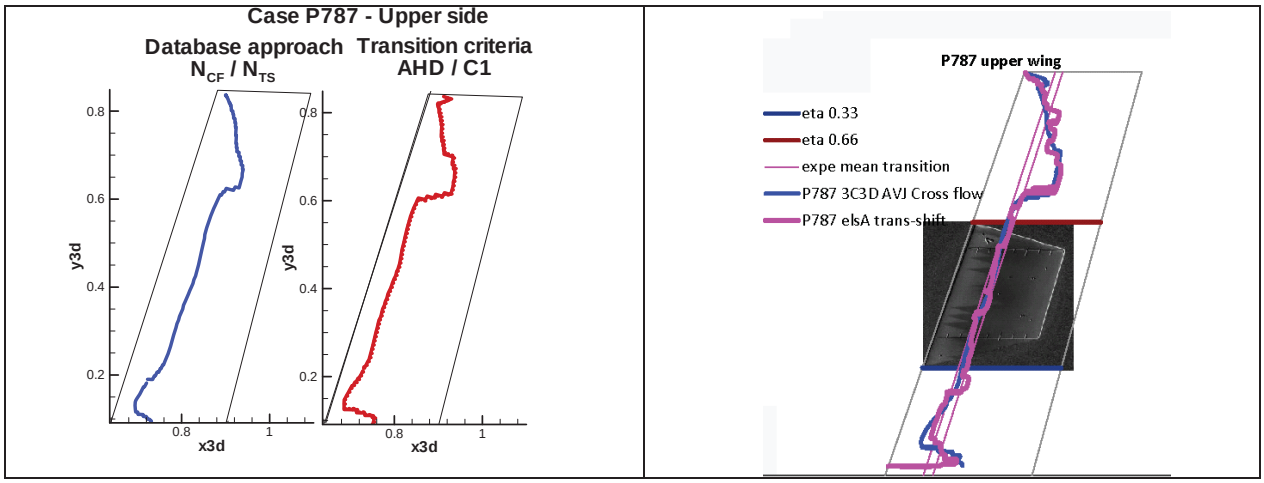


**Figure 23. Transition line computed on the Pathfinder wing, using 3C3D and transition prediction tools on the left side, and comparing to internal transition prediction in elsA on the right side.**

In general, very good comparisons are obtained in case of TS transition, while crossflow transition is not so well predicted: the C1 criterion is known to be less robust than other criterion based on the characteristics of the inflection point in the velocity profile. Further progress is needed in this regard.

Such computations require specific precautions when preparing the mesh, and require a longer computing time, but the increase was proved here to remain reasonable, with an increase of less than 30% in the number of iterations and a mesh that remain compatible with current 3D computations.

## V. Conclusion

After test Navier-Stokes mean flow numerical solutions were obtained for the Telfona Pathfinder model using the CFD++, DLR-TAU and elsA solvers. The Telfona Pathfinder model was designed, analyzed numerically, constructed and tested with the aim to obtain the capability of laminar flow testing in the ETW. The ETW test campaigns provided pressure distribution data and transition position obtained from images using the Cryogenic Temperature Sensitive Paint Method (CryoTSP). Stability analysis results were obtained using the $N_{TS}/N_{CF}$ local incompressible stability analysis method LILO. The numerical pressure distributions results verified the Pathfinder design requirement that the spanwise variation of pressure distribution is very small, even at off design conditions. This allows the use of stability analysis based on numerical or experimental pressure distributions from constant span sections. It is also shown that the Pathfinder pressure distribution is not sensitive to the use of turbulence models and either fixing transition or not. For comparison between numerical and experimental results, 10 cases from ETW Pathfinder test campaigns I and II were selected. The stability analysis based on ETW and CFD pressure distributions for these test cases shows good, in some cases very good agreement. Therefore CFD pressure distributions can be used to complement the analysis of the ETW test cases. Especially for the third Pathfinder test campaign this is very useful since no experimental pressure distributions exist.

Within the three Pathfinder test campaigns ETW´s capability for natural laminar flow testing improved. The CryoTSP imaging technique is proved to be an efficient method for transition detection. Besides the results obtained to demonstrate the capability and prepare ETW for laminar flow testing, the Pathfinder tests also showed some issues related to laminar boundary flow measurements which are general or particular to the Pathfinder test. It was observed that for predominant Tollmien-Schlichting transition in regions close to the nose, critical $N_{TS}$-factors seemed to correspond to free flight conditions. For the Pathfinder case turbulent wedges more frequently reduced the area with laminar boundary layer for predominant Tollmien-Schlichting cases, than for predominant cross-flow cases. The temperature step up and step down measurements performed in Phase III, indicate that the wall temperature seems to have a small effect, destabilizing or stabilizing the boundary layer. Analysis performed in this work did not take into account wall temperature effects because wall surface temperature distribution is unknown. An adiabatic wall temperature condition was assumed. The influence of wall temperature was considered for a special case in which TSP images were recorded in a temperature step up measurement. Specifying the wall temperature by reasonable assumptions, leads to results which reduce the fluctuations in correlated N-factors.

Validation of ONERA transition prediction tools embedded into the elsA RANS code were also presented.

At the extremely small boundary layer thickness which occurs for high Reynolds very tiny impurities lead to turbulent wedges. Therefore many TSP pictures do not show a clear transition line. Nevertheless, the complementary evaluation of numerical and experimental results has provided a total of 99 usable correlations for ETW test campaigns I and II. The stability analysis for ETW test campaign III, based on CFD-RANS provided an additional 33 usable correlations. These cases include critical $N_{CF}$, $N_{TS}$ values in regions of $N_{CF}$-$N_{TS}$ space not correlated neither in test campaigns I nor II. The stability analysis and the evaluation of pressure distributions allows a recommendation to be given for new flow conditions which in a further Pathfinder test could complete the determination of the critical $N_{CF}$-$N_{TS}$ boundary.

## Acknowledgments

The work presented in this paper may be considered as part of the research project TELFONA, performed under contract No. AST4-CT-2005-516109, financed by the European Union. Most of the work was performed after the project completion, motivated by the challenging database generated from the project. Special thanks are due to David Sawyers (Airbus) who was TELFONA Project coordinator and whose proofreading helped to improve this paper, to Fabien Dezitter, (Airbus), who contributed directly to the evaluation of the elsA capabilities, to Robert Houdeville (ONERA), who introduced the compressible version of the AHD criterion into elsA, to Winfried Kühn (Airbus) who contributed actively to the test, to Jean-Pierre Archambaud (ONERA) who was involved for the complete duration of the TELFONA project, to Paul White (Airbus) together with the ETW, DLR and Airbus team

of test engineers and technicians who prepared the model as well as planned, constructed and manufactured the Pathfinder model.

## References


[1]Schrauf, G., Horstmann, K.H. and Streit, T., "The Telfona Pathfinder Wing for the Calibration of the ETW Wind Tunnel". In Proceedings of the *1st CEAS European Air and Space Conference*, 10-13 September, Berlin, 2007.

[2]Fey, U., Egami, Y. and Engler, R.H. "High Reynolds number transition detection by means of Temperature Sensitive Paint", *AIAA Paper 2006-0514*, 2006.

[3] Perraud, J., Archambaud, J., Schrauf, G., Donelli, R., Hanifi, A., Streit T., Hein, S., Fey, U., Egami, Y., "Transonic High Reynolds Number Transition Experiments in the ETW Cryogenic Wind Tunnel". *AIAA Paper 2010-1300, 48th AIAA Aerospace Sciences Meeting*, 04.-07. Jan. 2010, Orlando, Fl., USA, 2010.

[4] Perraud, J., Salah El Din, I., Schrauf, G., Hanifi, A., Donelli, R., Hein, S., Fey, U., Egami, Y., Streit T., **"**High Reynolds Number Transition Experiments in the ETW Test Facility with the Pathfinder Model". *Proccedings of the V European Conference on Computational Fluid Dynamics*, ECCOMAS CFD 2010 , Lisbon, Portugal, 2010.

[5]G. Schrauf, K.H. Horstmann, T. Streit, J. Perraud, and R. Donelli, "The Telfona Pathfinder Wing for the Calibration of the ETW Wind Tunnel" KATnet II *Conference on Key Aerodynamic Technologies*, 12-14 May, Bremen, 2009.

[6]Streit, T., Schrauf, G., Salah El Din, I., Cella, U., Fey**,** U.**,**Egami, Y. **"**The Telfona Pathfinder Model a Second Look" *Proccedings of the V European Conference on Computational Fluid Dynamics*, ECCOMAS CFD 2010 , Lisbon, Portugal, 2010.

[7]Kroll, N., Fassbender, J.K., "MEGAFLOW – Numerical Flow Simulation for Aircraft Design, *Notes on Numerical Fluid Mechanics and Multidisciplinary Design (NNFM), 89*", Springer Verlag, Closing Preparation DLR Project MEGAFLOW, 2002 Braunschweig, 2002.

[8]Peroomian, O. and Chakravarthy, S., "A 'Grid-Transparent' Methodology for CFD," In *AIAA Paper No. 97-0724*, Reno 1997.

[9] Gazaix, M., Jollès, A., Lazareff, M., "The elsA Object-Oriented Computational Tool for Industrial Applications". 23rd ICAS Congress, Toronto (Canada), September 2002.

[10]Schrauf, G., "LILO 2.1 – Users "Guide and Tutorial", GSSC Technical Report, July 2006.

[11]Laburthe, F., "Problème de stabilité linéaire et prévision de la transition dans des configurations tridimensionnelles, incompressibles et compressibles", *Thèse de Doctorat Sup'Aéro*, Toulouse, Dec. 1992.

[12]Casalis, G., Arnal, D., "ELFIN II, Subtask 2.3: Data Base Method. Development and Validation of the Simplified Method for Pure Crossflow Instability at Low Speed" ELFIN Technical Report Nb145, 1996.

[13] Perraud, J., Arnal, D., Casalis, G. and Donelli R., "Automatic Transition Predictions using Simplified Methods", AIAA Journal, Vol. 47, No. 11, Nov. 2009, pp 2676-2684, doi: 10.2514/1.42990

[14] Krimmelbein, N., Radespiel, R., "Transition Prediction for Three-Dimensional Flows Using Parallel Computation". Computers & Fluids, 38, pp. 121-136, 2009.

[15] Arnal D., "Three-dimensional boundary layers: laminar-turbulent transition", Special Course on « Computations of three-dimensional Boundary Layers including Separation », VKI, AGARD Report 741, 1986.

[16] Krimmelbein, N., Krumbein, A., "Automatic Transition Prediction for Three-Dimensional Configurations with Focus on Industrial Application". *AIAA Paper 2010-4292, 40th AIAA Fluid Dynamics Conference and Exhibit*, Chicago, USA, 2010.

[17] Cliquet, J., Houdeville, R., and Arnal, D., "Application of Laminar-Turbulent Transition Criteria in Navier-Stokes Computations", AIAA Journal, Vol. 46, No. 5, 2008, pp.1182-1190. doi: 10.2514/1.30215

[18]Schwamborn, D., "Laminare Grenzschichten in der Nähe der Anlegelinie an Flügeln und flügelähnlichen Körpern mit Anstellung". DFVLR-FB 81-31, 1981.

[19]Hein, S., Bertolotti, F.P., Simen, M., Hanifi, A., Henningson, D., "Linear Nonlocal Instability Analysis – the linear NOLOT code-", DLR-IB 223-94 A56, 1994.

[20]Redeker, G.,Wichmann, G., "Forward Sweep - a Favourable Concept for Laminar Flow". In Journal of Aircraft, Vol. 28, No. 2, pp. 97-103, 1991.